Semi-flexible immunobrushes facilitate effective and selective expansion of antigen-specific T cells

Gerrits, L.; Weiss, L.; Grad, E.M.; Schluck, M.; Maassen, L.; Classens, R.; ... ; Hammink, R.

ADVANCED FUNCTIONAL MATERIALS
www.afm-journal.de

Semi-Flexible Immunobrushes Facilitate Effective and Selective Expansion of Antigen-Specific T Cells

Lotte Gerrits, Lea Weiss, Emilia M. Grad, Marjolein Schluck, Lisa Maassen, René Classens, Chadia Archidi, Martijn Verdoes, Carl G. Figdor, Paul H. J. Kouwer,* and Roel Hammink**

Adoptive T cell therapy (ACT) has achieved remarkable results in the treatment of cancer. Tumor-antigen specific T cells are the main players in the clearance of cancerous cells, but generating large numbers is a major hurdle in clinical practice. One shortcoming of current expansion procedures is that the artificial presentation of T cell activating signals on rigid surfaces do not recapitulate the physiological presentation on a fluidic membrane. To address this, semi-flexible poly(isocyanopeptide) (PIC) immunofilaments (IFs) are generated coated on micro-sized magnetic beads (immunobrushes (IB)). IBs are functionalized with peptide-loaded major histocompatibility complexes (pMHC, signal 1) and agonistic anti-CD28 antibodies (αCD28, signal 2) to effectively expand and enrich antigen-specific T cells. As a direct result of the immunobrush design, strong T cell activation and excellent tumor cell killing capacities are found. More importantly, high selectivity is demonstrated by strong expansion and enrichment of antigen-specific T cells in a pool of non-specific cells (93-fold enrichment of antigen specific T cells in 7 days). The modular character of the immunobrush-based strategy makes it a great platform for highly effective ACT-based therapies.

1. Introduction

In the past decade, ACT has shown promising results toward the treatment of cancer.[1] This therapy involves administration of ex vivo activated immune cells, such as tumor infiltrating lymphocytes (TILs), autologous tumor-specific T cells or T cells equipped with a modified receptor such as chimeric antigen receptor (CAR)-T or engineered T cell receptor (TCR)-T cells. Various clinical trials have demonstrated the great potential of ACT for the treatment of melanoma.[2] To generate sufficient doses of effective tumor-specific T cells, production of antigen-presenting cells (APCs) is required,[3] which, however is expensive and time-consuming and may lead to quality variation in the ex vivo generated T cells.[4] To circumvent these issues, artificial antigen-presenting cells (aAPCs) have been developed as an "off-the-shelf" platform for expansion of T cells.[5] Of the different aAPCs approaches, Dynabeads (DyBs) have become the gold standard. These clinically approved rigid beads are functionalized with antibodies: agonistic CD3 (αCD3) for T cell receptor stimulation, and αCD28 for co-stimulation in combination with exogenous supply of Interleukin-2 (IL-2).[6] For (antigen-specific)T cell stimulation, DyBs have two major disadvantages: the rigid and non-natural presentation of the signals on the beads does not comply with TCR rearrangement, which can lead to suboptimal stimulation; due to the rigid, non-natural presentation of the signals,[7] and

L. Gerrits, P. H. J. Kouwer
Institute for Molecules and Materials
Radboud University
Heyendaalseweg 135, Nijmegen 6525 AJ, The Netherlands
E-mail: P.Kouwer@science.ru.nl

L. Gerrits, L. Weiss, M. Schluck, M. Verdoes, C. G. Figdor, P. H. J. Kouwer
Institute for Chemical Immunology
Nijmegen 6525 GA, The Netherlands
E-mail: Carl.Figdor@radboudumc.nl

L. Weiss, E. M. Grad, M. Schluck, L. Maassen, R. Classens, C. Archidi, M. Verdoes, C. G. Figdor, R. Hammink
Department of Medical BioSciences
Radboudumc
Geert Grooteplein 26, Nijmegen 6525 GA, The Netherlands
E-mail: Roel.Hammink@radboudumc.nl

L. Weiss, M. Schluck, C. G. Figdor, R. Hammink
Division of Immunotherapy
Oncode Institute
Radboud University Medical Center
Nijmegen 6525 GA, The Netherlands

The ORCID identification number(s) for the author(s) of this article can be found under https://doi.org/10.1002/adfm.202307606

DOI: 10.1002/adfm.202307606

they stimulate T cells polyclonally, i.e., non-specifically, which can lead to off-target toxicity.[8]

Alternatives that have been prepared to allow clustering of the nanoscale TCR structures on the surface of naive T cells[9] to micron-sized aggregates that initiate and sustain T cell activation,[10] include lipid bilayers or aAPCs with pre-clustered signals.[7a,9–11] The large majority of these platforms, however, do not carry antigen-specific T cell activating signals, which, analogous to DyBs, yields polyclonal activation. Here, we introduce aAPCs that effectively stimulate antigen-specific T cells and allow for TCR rearrangement.

Our aAPC is based on a bead-immobilized PIC scaffold. The semi-flexible nature of the PIC scaffold can present T cell activating signals in a physiological representative manner and can allow rearrangement of the formed ligand-receptor complexes to facilitate TCR clustering.[11e,f,12] In earlier work, PICs were decorated with αCD3 and αCD28 or IL-2 to afford IFs. These IFs showed high T cell activation and expansion efficiency.[11e,f] Grafting the IFs to a magnetic microbead yields IBs and introduces easy handling and straightforward separation from the T cell cultures.[11g] The IBs effectively induced polyclonal activation and expansion of human pan T cells that outperformed DyBs and other commercially available aAPCs.[11g]

In this paper, we created IBs to expand antigen-specific $CD8^+$ T cells through improved aAPC–T-cell interactions. After determining optimal densities of T cell activation signals (pMHC and αCD28) for murine OT-I T cells, we establish that IBs more effectively expand T cells than corresponding beads with the activation signals bound directly to the particle core. Additionally, we demonstrate that our IBs enrich antigen-specific OT-I T cells within a population of non-specific T cells (after 13 days in culture, the population increased from 10% to 99%) or in a pool of splenocytes. Expanded cells were highly functional and showed limited signs of exhaustion. These findings demonstrate the great potential of our IB platform as an effective aAPC that facilitates enrichment and expansion of rare tumor antigen-specific T cells ex vivo.

2. Results and Discussion

2.1. Synthesis and Characterization of Immunobrushes

Antigen-specific T cell activating IBs were prepared by grafting PIC polymers to micrometer-sized beads, via an adaptation of a previously described procedure (**Figure 1a**).[11g,13] Due to the semi-flexible character of the PIC, access to substituents on the polymer chain is ensured,[14] which makes PICs an attractive scaffold for the development of T cell activation platforms. We synthesized PIC block-copolymers that comprise a first block of 100 allyl- and methoxy-functionalized monomers in a 0.5:0.5 ratio and second block of 2000 azide- and methoxy-functionalized monomers in a 0.03:0.97 ratio. The allyl and azide handles facilitate orthogonal post functionalization of the polymer scaffold (Figure 1b). The average length of the PIC block-copolymer was 219 nm, with a polydispersity index of 1.25, which was determined using atomic force microscopy (AFM) (Figure S1a,b, Supporting Information). The average molecular weight of the polymers was found to be 687 kg mol^{-1}. To obtain IFs, PICs were functionalized via a two-step protocol. The first block was modified with a biotin linker via a nitrile-imine mediated cycloaddition (NITEC) reaction between the allyl groups on the polymer chain and the tetrazole ring in the biotin-linker (Figure 1c). Subsequently, the azide groups in the second block of the PIC chain enabled conjugation of dibenzocyclooctyne (DBCO)-modified fluorescently labeled immunomodulators (DBCO-SIINFEKL-pMHC, -αCD28, and -IL-2, Table S1, Supporting Information) via strain promoted alkyne-azide cycloaddition (SPAAC) (Figure 1d). As the optimal size range for aAPCs was previously found to be 4 to 5 µm[15], we used tosyl-activated microbeads with a diameter of 4.5 µm and coated these with streptavidin to afford IBs by grafting the IFs through biotin-streptavidin interactions.

Confocal laser scanning microscopy (CLSM) confirmed the successful grafting of the IFs on the microbeads (Figure 1e). The immunomodulator concentration per IB type was determined via flow cytometry. The fluorescent labels on each immunomodulator enabled us to correlate the mean fluorescent intensities (MFI) of the IBs to standard curves that were generated via a so-called stripping assay (Experimental Section, Synthesis of Immunobrushes and Direct Beads) where all signals are cleaved from the beads.[13] An overview of all IB types and their immunomodulator concentrations can be found in Table S2 (Supporting Information).

2.2. Immunobrushes Require Co-Stimulatory Signal αCD28 for Optimal Interaction with OT-I T Cells

To determine the minimal required signals for antigen-specific T cell activation, we used primary transgenic $CD8^+$ OT-I T cells. OT-I T cells recognize the SIINFEKL-peptide, a dominant epitope of the ovalbumin protein, which is presented on the MHC-I complex. To test T cell activation, we decorated IBs with IF-pMHC, IF-pMHC/αCD28, IF-pMHC/αCD28/IL-2, and IF-αCD28/IL-2 (**Figure 2a**). After one day of incubation, OT-I T cells and IBs with αCD28, pMHC, and/or IL-2 clustered, which increased on day 2 and 4 (Figure 2b). The presentation of pMHC alone did not induce such visible interaction between OT-I T cells and IBs, while the presentation of both αCD28 and IL-2 without pMHC led to some cluster formation. IBs comprising IF-pMHC/IL-2 were not taken along as we observed that addition of αCD28 was required for sufficient interaction with OT-I T cells. As the level of T cell clustering may not directly relate to the degree of stimulation, we evaluated the proliferation and cytokine secretion as indicators of stimulation of T cells.

The IBs presenting both pMHC and αCD28 induced a higher division index (3.7 cycles) compared to IBs presenting pMHC only (0.4 cycles) or IBs presenting αCD28 and IL-2 (0.1 cycles) (Figure 2c; Figure S3a–c, Supporting Information). After stimulation with IF-pMHC/αCD28 IBs, we observed increased secretion of IFNγ, IL-2, and TNFα (138.4, 33.4, 10.3-fold, respectively) compared to unstimulated OT-I T cells (Figure 2d,e; Figure S3d–f, Supporting Information). The addition of IL-2 to IBs presenting pMHC and αCD28, either immobilized on IFs or soluble, did neither lead to a significantly higher division index, nor to higher cytokine secretion (Figure 2c–e; Figure S3a–f, Supporting Information). DyBs induced proliferation to similar levels as IF-pMHC/αCD28 IBs, but lower cytokine secretion (Figure S3a–f,

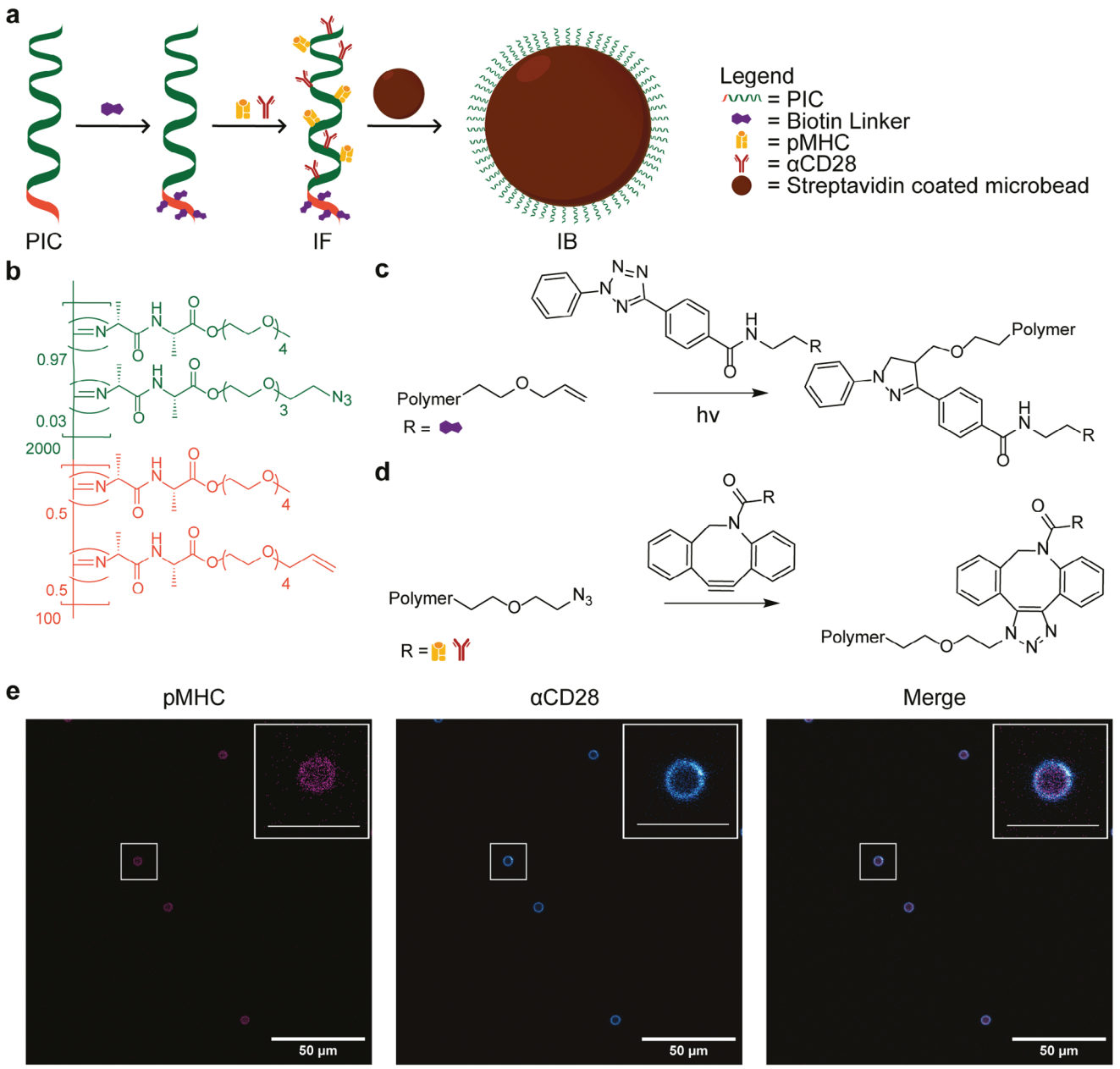

Figure 1. Synthesis of IBs. a) Schematic overview of the preparation of IBs; PIC is biotinylated, followed by conjugation of the Immunomodulators and subsequent grafting of the IFs to streptavidin-coated microbeads. b). Chemical structure of PIC. c) Overview of the NITEC reaction that is used to conjugate a biotin linker to PIC via reaction between the allyl groups in the first block of the polymer chain and the tetrazole ring in the biotin linker. d) Overview of the SPAAC reaction that is used to conjugate Immunomodulators to PIC via click reaction between the azide groups in the second block of the polymer chain and the DBCO-moieties on the immunomodulators. e) CLSM images of IBs with pMHC and αCD28. Scale bar is 50 µm. Inset scale bar is 12.5 µm.

Supporting Information). Our findings indicate that both pMHC and αCD28 are required for robust T cell activation. pMHC triggers TCR-mediated T cell activation, while αCD28 supports IB-T cell interaction and likely provides a co-stimulus that further boosts T cell activation, which cannot further be enhanced with IL-2 presentation. It is possible that our IBs presenting pMHC and αCD28 already induce maximum stimulation of OT-I T cells.

To assess how quantity and density of antigen and co-stimulation presented to T cells can influence their activation,[16] we continued optimization by varying the density of pMHC and αCD28-functionalized IFs on the beads, as well as the bead to cell ratio (Figure 2f; and Table S2, Supporting Information). We found that OT-I T cell activation was dependent on both IF density and the bead to cell ratio (Figure 2g,h). **IB1**, presenting the

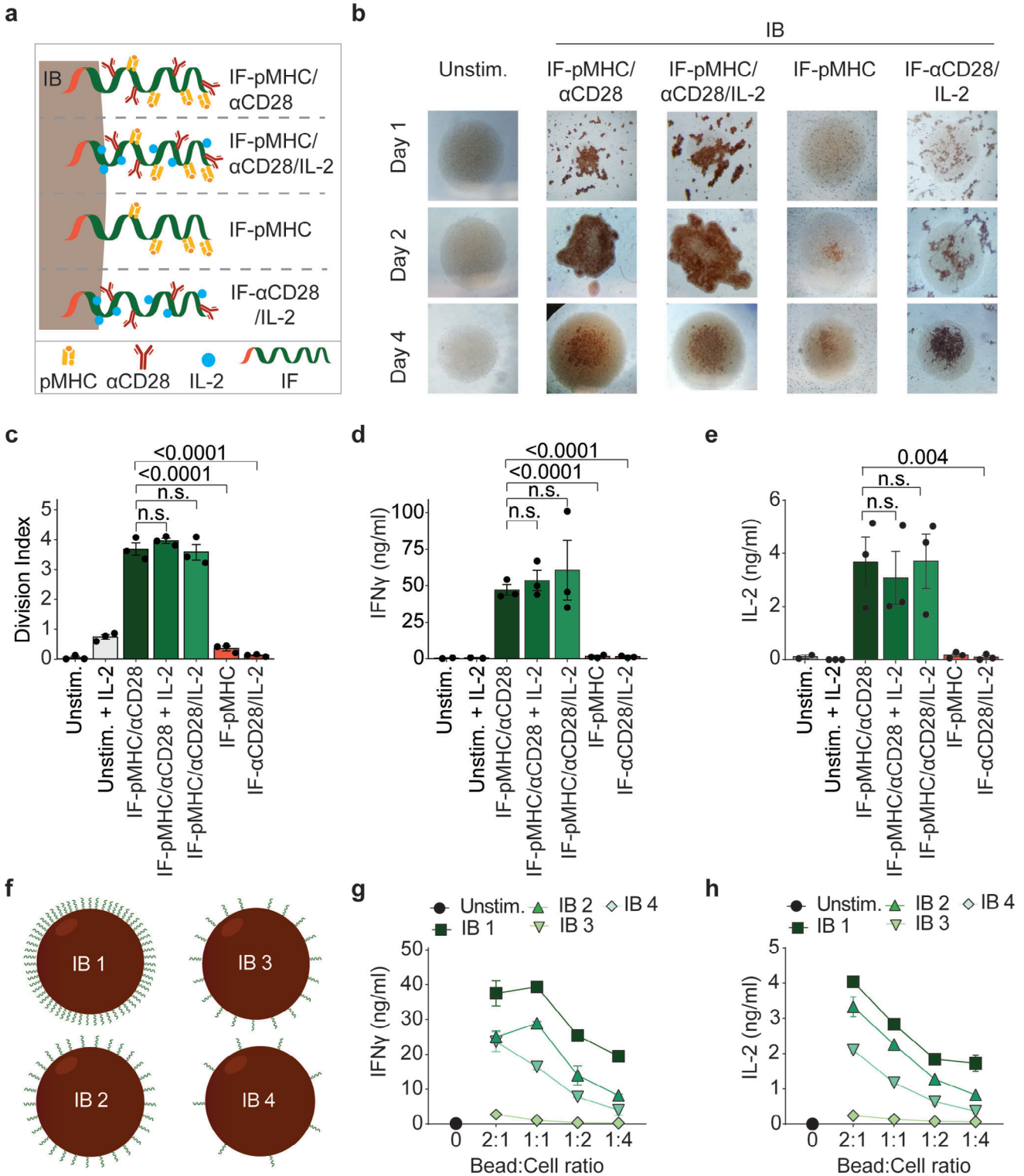

Figure 2. Activation of CD8$^+$ OT-I T cells depends on the type of IB, IF density, and IB to cell ratio. a) Illustration of IFs with different immunomodulators (pMHC, αCD28 and IL-2) coupled on a magnetic bead to generate IBs. b) Brightfield microscopic images of cultured OT-I T cells (transparent) with IBs (brown) on day 1,2 and 4. c–e) Division index on day 4 c) and cytokine secretion on day 2 d,e) of cultured OT-I T cells. f) Illustration of **IB1-4**: magnetic beads coated with different densities of IF-pMHC/αCD28. IF density decreases from **IB1** to **IB4**. The illustration does not represent the real IF density on the beads. g,h) Effect of IF density and bead to cell ratio on OT-I T cell cytokine secretion. Data was analyzed with one-way ANOVA on log-transformed data (c-e) with post-hoc Sidak's multiple comparison test. The p-values are indicated for relevant comparisons. n = 2-3 in one or three independent experiments.

highest IF density resulted in a 36.8-fold higher IFNγ secretion and a 21.1-fold higher IL-2 secretion when compared to **IB4**, presenting the lowest IF density at a 1:1 bead: cell ratio (Figure 2g,h). **IB2** and **IB3** coated with an intermittent IF density, led to lower cytokine secretion than **IB1**, but higher cytokine secretion than **IB4**. At a 1:1 ratio, **IB1** presents ≈4.1 ng pMHC to the cells in culture, while **IB4** presents only 0.34 ng pMHC, which likely explains the higher secretion achieved with **IB1**. When we varied the bead concentration and IF density to match the pMHC concentration (**IB2**, 1:2 bead:cell ratio with 0.76 ng pMHC and **IB4** at a 2:1 bead cell ratio with 0.68 ng pMHC), we observed an increase in IFNγ (5.1-fold) and in IL-2 production (5.3-fold) for **IB2** (Figure S3g–i, Supporting Information), which indicates that both the total and the local density of pMHC play a role in T cell stimulation. From these results, we observe that OT-I T cells are effectively stimulated by IBs with IF density similar to **IB2**. In addition, the preparation of **IB1** required 4 times more IFs than **IB2**, which makes **IB2** a more favorable design. We thus selected beads similar to **IB2** and a 1:1 bead to cell ratio as the optimal setting for all subsequent experiments.

2.3. pMHC and αCD28 Presented via Immunobrushes are Superior to Rigid Bead Surfaces for Stimulating OT-I T Cells

To investigate whether IFs have a beneficial effect on T cell activation, we generated beads with matching amounts of pMHC and αCD28 directly attached to the surface of the beads (DirectB, Table S2, Supporting Information). While the fraction of OT-I T cells that express the early activation marker CD25 is similarly high for IBs (99.9%) and DirectBs (94.2%, Figure S4a, Supporting Information), the overall expression is much higher (7.2-fold) for IBs (**Figure 3**a,b). The early activation marker CD69 showed a similar trend (Figure S4b,c, Supporting Information). IBs induced 5.9-fold higher IFNγ and 11-fold higher IL-2 secretion compared to DirectBs (Figure 3c,d). These results corroborate our previous finding where αCD3/αCD28 decorated IBs outperformed matching DirectBs by inducing higher cytokine secretion of human pan T cells.[11g] We confirm that presenting immunomodulators on IFs has an advantage over directly grafted immunomodulators, which we tentatively attribute to the presence of the filaments that allow receptor rearrangements and support multivalent interactions.[11e] Next, we compared our platform to natural APCs , such as dendritic cells (DCs) pulsed with SIINFEKL. Interestingly, IB- and DC- stimulated OT-I T cells showed similar levels of CD25 expression (Figure 3e,f) and IFNγ, two days after incubation (Figure 3g). DCs induced slightly, but not significantly, higher levels of IL-2 secretion compared to IBs (Figure 3h). This finding indicates that initial T cell activation induced with IBs is equally strong to the one provoked by natural DCs.

For ACT, T cells are expanded for several days up to weeks to reach sufficient numbers. During this expansion period, prolonged stimulation can lead to exhaustion of T cells, which renders them incapable of lysing tumor cells.[3,17] Hence, it is important to determine whether IB-expanded OT-I T cells preserve their cytotoxic abilities. To this end, we expanded OT-I T cells for two weeks with IBs and soluble IL-2 (Figure 3i; Figure S4d,e, Supporting Information). DirectB, DC and DyB expanded OT-I T cells were taken along as controls. We used an ovalbumin antigen-expressing B16 tumor cell line ($B16^{OVA}$) as target cells. Following magnetic removal of IBs and sorting of $CD8^+$ cells, OT-I T cells were co-cultured with $B16^{OVA}$ and OVA-negative B16 cells. When expanded with IBs, OT-I T cells lysed 68.2% $B16^{OVA}$ cells in a 4:1 effector: target ratio, while unstimulated OT-I T cells only reached 11.4% (Figure 3j). Even at a 1:2 ratio, 28.5% $B16^{OVA}$ cells were lysed by IB-stimulated OT-I T cells (Figure 3j). Only at very high, 4:1 effector: target ratios, ≈22% of the OVA-negative B16 cells were lysed, likely due to non-specific cytotoxicity of IB-activated OT-I T cells (Figure 3k).[18] Thus, we demonstrate that T cells can be expanded by IBs over a prolonged period of time, while preserving their ability to kill antigen-expressing target cells. DirectB-, DC- and DyB- expanded OT-I T cells showed similar abilities to lyse $B16^{OVA}$ cells (59.1%, 52.4%, 65.6% lysis, respectively at 4:1 ratio) or OVA-negative B16 cells (18.4%, 22.7%, 25.3% lysis, respectively at 4:1 ratio) (Figure S4d,e, Supporting Information). Because the same number of activated OT-I T cells were added to the target cells for each condition, it was expected that all conditions showed similar killing abilities. We demonstrate that IBs stimulate OT-I T cells more effectively, yet DirectBs, DCs and DyBs are also capable of activating OT-I T cells. As a result, the subsequent killing assay shows the effectiveness of the expanded cells from all conditions to lyse target cells.

2.4. Immunobrushes Induce Antigen-Specific Proliferation of OT-I T Cells and Enrich OT-I T Cells in a Pool of Non-Specific Wildtype $CD8^+$ T Cells

The success of T-cell based immunotherapy relies on the ability to expand tumor antigen-specific T cells.[19] Given the need for an effective and easily applicable platform for antigen-specific T cell expansion, we tested whether IBs are an effective tool to expand antigen-specific T cells from a pool of non-specific T cells. To do so, we mixed 10% of dsRed-expressing $CD8^+$ OT-I T cells into a pool of non-specific wildtype $CD8^+$ T cells (**Figure 4**a). The expression of the red fluorescent protein (dsRed) in OT-I T cells allows to easily distinguish them from non-specific cells, particularly when OT-I T cells are present in low numbers. We found that OT-I T cells clustered with IBs (Figure 4b), while they were evenly distributed in the culture wells with DyBs. After three days, we observed that IBs induced proliferation in OT-I T cells (3.7 cycles), but not in non-specific T cells (0.1 cycles) (Figure 4c,d; Figure S5a, Supporting Information). As expected, DyBs stimulated both non-specific T cells and OT-I T cells, which both had an average cycle of 1.4. (Figure 4d; Figure S5a,b, Supporting Information). The lower overall proliferation rate observed with DyBs is likely due to a competition for activation signals by all cells in the culture and possibly a higher consumption of nutrients that can impact expansion of both OT-I and non-specific T cells (Figure S5f, Supporting Information).[20] After 7 days of expansion with the IBs, we observed a 5.3-fold expansion of OT-I T cells, which increased to 20.4-fold on day 13 (Figure 4e,f; Figure S5c, Supporting Information). DyB-stimulated T cells showed no or only minor expansion. Strikingly, IBs could specifically expand OT-I T cells, when only 1%, 0.1%, and even when 0.01% of the starting populations consisted of OT-I T cells, although the low cell count induces a larger

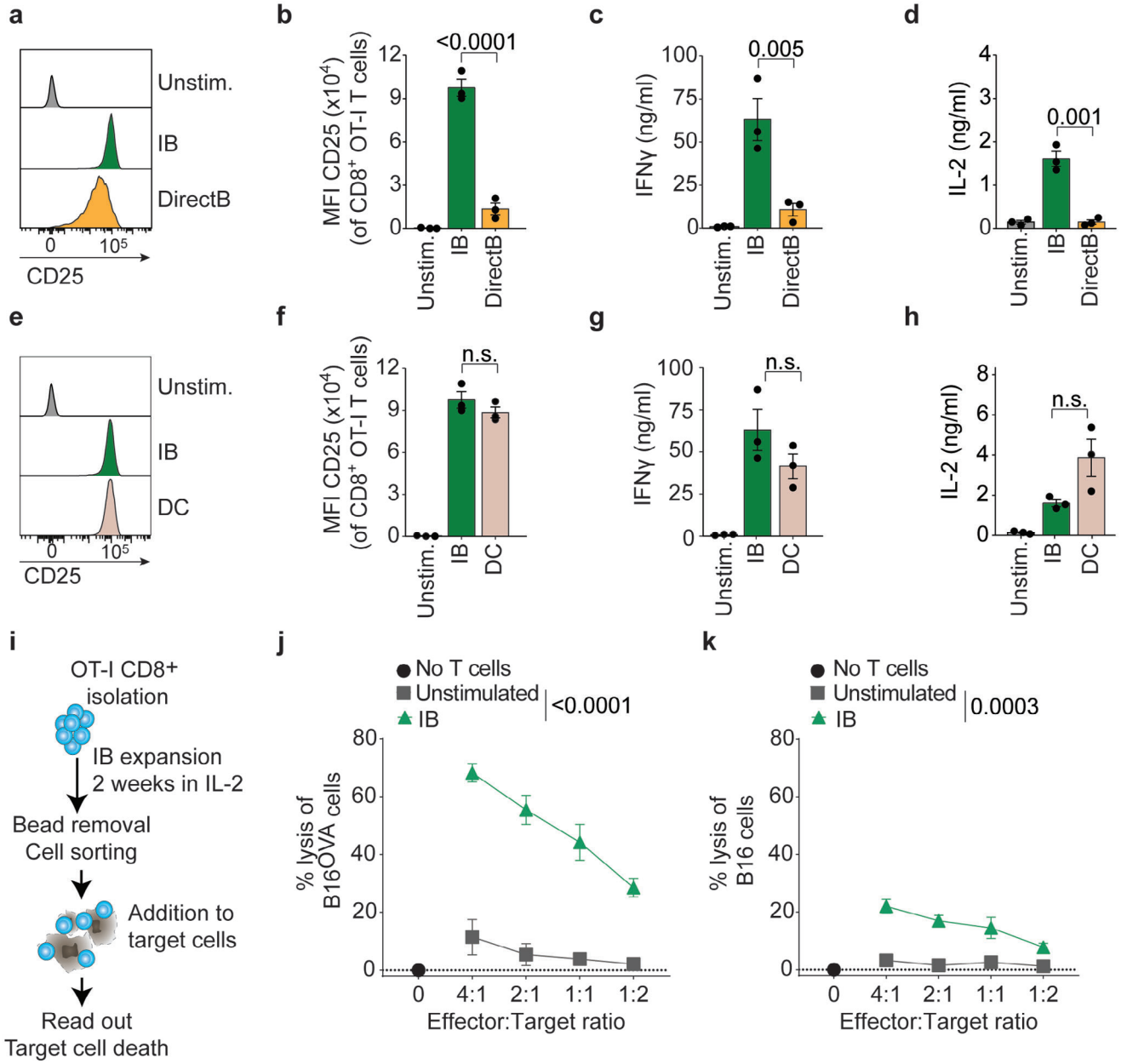

Figure 3. Comparison of OT-I CD8$^+$ T cell activation with IBs, DirectBs and DCs. a–d) OT-I T cells were stimulated with IBs or DirectBs with matching amounts of pMHC and αCD28 in a 1:1 bead tocell ratio. a) Histograms illustrate CD25 expression b), which is quantified after 2 days of culture. c,d) Cytokine secretion was measured after two days by ELISA. e–h) OT-I T cells were stimulated with IBs presenting IF-pMHC/αCD28 in a ratio of 1:1, or with Flt3 Ligand DCs at a ratio of 5 OT-I cells to 2 DCs for two days. e,f) Flow cytometric read out of CD25 expression as histogram of one representative donor e) or quantified relative expression f). Cytokine secretion was assessed by ELISA g,h). a–h) Experiments were performed at the same time and are only split up for demonstrative purposes. i) Expansion protocol with IBs for OT-I T cell expansion. j,h) Percentage of specific lysis of B16^{OVA} target cells (i) or non-target OVA-negative B16 cells j) at indicated effector to target ratios by sorted OT-I CD8$^+$ T cells that were expanded for two weeks. Statistical significance was tested with one-way ANOVA on non-transformed (b,f) or log-transformed (c,d,g,h) data with post-hoc Sidak's multiple comparison test or two-way ANOVA j,k) with post-hoc Tukey's multiple comparison test. n = 3-4 in one or two independent experiments.

variation across different experiments (Figure S5c, Supporting Information). When stimulated with IBs, we observed a significant enrichment of OT-I T cells on day 7 (92.3% of the whole population) that increased further to almost exclusively OT-I T cells on day 13. Enrichment of antigen-specific T cells was also observed in cultures with lower starting frequencies of OT-I T cells (Figure S5d,e, Supporting Information). In contrast, stimulation with DyBs yielded an OT-I T cell population close to the starting population of 10% (12.2% day 7, 13.5% day 13) (Figure 4g,h; Figure S5d,e, Supporting Information).

To learn more of the proliferative capacity and effector function of the cells, we assessed the phenotype of the OT-I T cells after

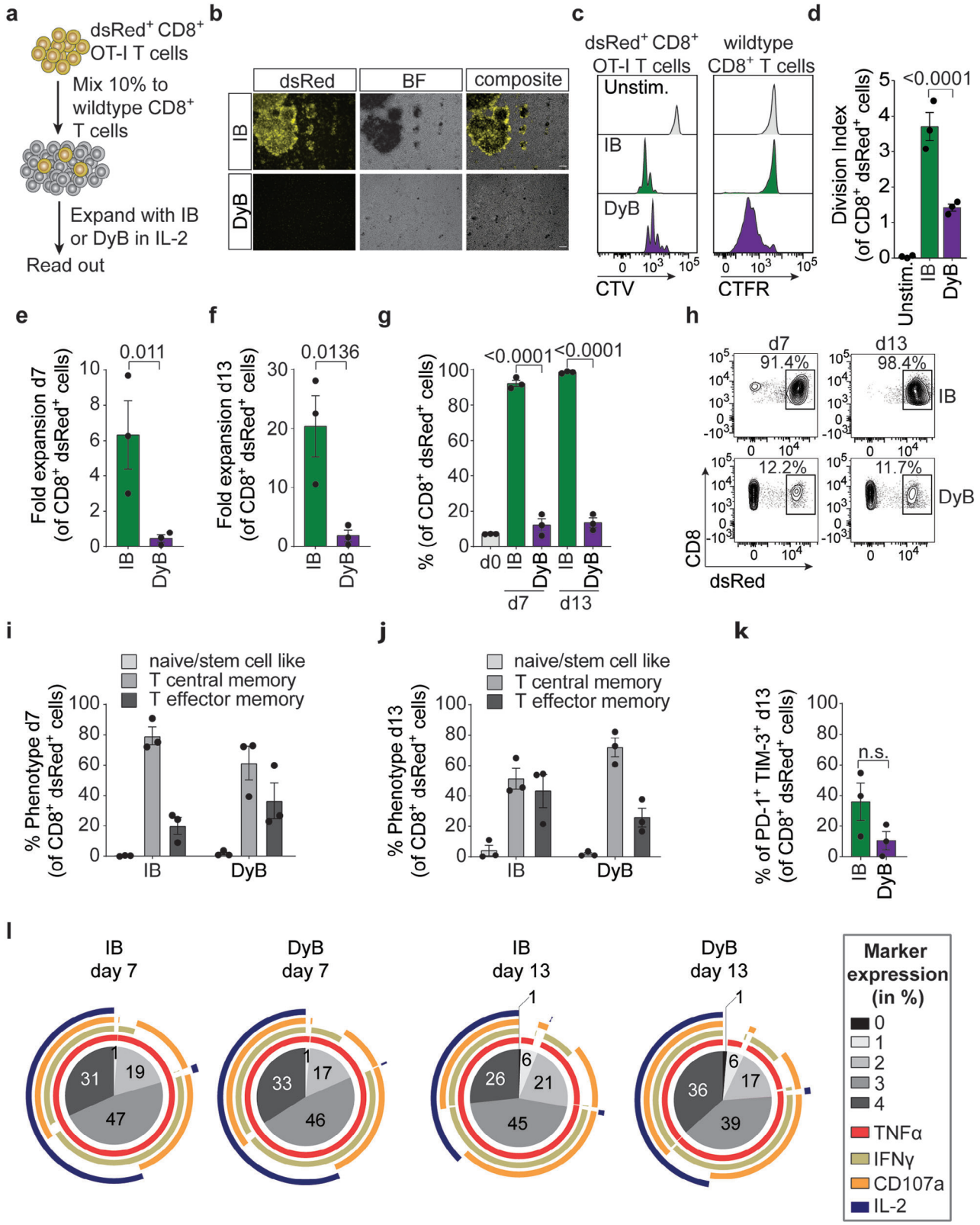

Figure 4. IBsspecifically expand and enrich functional antigen-specific CD8+ T cells. a) Schematic work-flow of expansion protocol. b) Epi-fluorescent and bright-field (BF) image and composite image of dsRed+ OT-I T cells (yellow) and beads (black) within the wildtype T cell population. c) Histogram representing proliferation tracer CTV dilutions of OT-I T cells and CTFR dilutions of wildtype T cells after 4 days of stimulation. d) Division index of OT-I T cells after 4 days of stimulation with either IBs or DyBs or left unstimulated (Unstim.). e,f) Fold expansion from starting population on day 7 e) and day

7 and 13 days of stimulation (Figure S6a, Supporting Information). We note that a T central memory phenotype (T_{cm}) is associated with a higher proliferative capacity, a T effector memory phenotype (T_{em}) represents cells with a higher effector function.[21] After 7 days of IB stimulation, 79.2% of the OT-I T cells showed a central memory phenotype and 20.8% an effector memory phenotype (Figure 4i; Figure S6b, Supporting Information). On day 13, the effector phenotype increased toward 43.3%, while 51.3% of the OT-I T cells were T_{cm} (Figure 4j; Figure S6c, Supporting Information). In comparison, DyBs generated more OT-I T cells with a T_{cm} phenotype (61.4% on day 7 and 71.9% on day 13) (Figure 4i,j; Figure S6d,e, Supporting Information). These differences in phenotype may be a direct result of the number of beads, thus stimulators, available per cell. This indicates that the phenotype can be influenced by the number of IBs given which can have implications for the future design of expansion protocols (Figure S6b,c, Supporting Information). Underlining this notion, we observed similar proportions of T_{cm} and T_{em} between 0.01% and 10% conditions when the OT-I T cells were stimulated with DyB (Figure S6d,e, Supporting Information).

Besides the T cell phenotype, we also investigated exhaustion levels by measuring the expression of the markers PD-1 and TIM-3. On day 13, ≈36% of IB stimulated OT-I T cells showed expression of both exhaustion markers, while only 11% of DyB-stimulated OT-I T cells had this phenotype (Figure 4k; Figure S6f–m, Supporting Information). Despite higher expression of exhaustion markers upon IB stimulation, OT-I T cells remained multifunctional as evident by the co-expression of the effector molecules IFNγ, TNFα, IL-2, and CD107a upon restimulation. We found that the majority of OT-I T cells stimulated with IBs remained multifunctional, as 76% on day 7 and 69% on day 13, still expressed 3 or 4 of these markers (Figure 4l; Figure S7b–i, Supporting Information). Similar multifunctionality was found for DyB-stimulated OT-I T cells (79% on day 7, 73% on day 13) (Figure 4l; Figure S7b–i, Supporting Information). Together with our results from the killing assay (Figure 3j,k), we conclude that our IBs selectively enrich and expand highly functional antigen-specific $CD8^+$ T cells even when precursor frequencies are low.

2.5. Immunobrushes Effectively Enrich and Expand Adoptively Transferred OT-I T Cells in a Pool of Splenocytes

Given these encouraging results, we wanted to confirm that we can selectively expand rare subsets in a diverse cell population with our IBs. To this end, we adoptively transferred $1{\cdot}10^6$ $CD45.2^+$ $CD8^+$ OT-I T cells into $CD45.1^+$ wildtype mice (**Figure 5a**). After 4 or 5 days, splenocytes were isolated. The starting population of OT-I T cells in the spleen was on average 0.3%. After 7 days of incubation in either IL-2 (Figure 5; Figure S8, Supporting Information) or IL-7 (Figure S9, Supporting Information) with IBs or DyBs, we assessed the enrichment and expansion, phenotype, exhaustion and multifunctionality of the OT-I T cells (Figure S8a, Supporting Information). With the IL-2 protocol, IBs enriched OT-I T cells on average 93-fold from the starting population within 7 days (Figure 5b,c); in contrast, DyBs only facilitated a 10-fold enrichment from the starting population. Additionally, IBs yielded an average fold expansion of 77-fold OT-I T cells, which was higher compared to DyBs (68-fold expansion) (Figure 5d). This result corroborates our previous findings and highlights that our IBs efficiently enrich and expand antigen-specific T cells in a pool of non-specific cells.

After 7 days, the majority of IB-treated and DyB-treated OT-I T cells (62% and 65%, respectively) had a T_{em} phenotype (Figure 5e; Figure S8b, Supporting Information). Accordingly, 38% of IB- and 33% of DyB-treated OT-I T cells had a T_{cm} phenotype. Furthermore, we found that the majority of the unstimulated $CD45.1^+$ T cells also had a T_{em} phenotype (Figure S8t, Supporting Information) when treated with IL-2. It is worth noting that upon stimulation in IL-7, most of the IB- and DyB-treated OT-I T cells had a T_{cm} phenotype (68% and 72%, respectively), while respectively 31% and 22% had a T_{em} phenotype (Figure S9c, Supporting Information), which demonstrates that the added cytokine plays a role in dictating the phenotype of the cells. Although ACT products that have a higher proportion of T_{cm} phenotype are associated with better tumor control in vivo,[22] it is worth considering that in these experiments IBs generated an overall higher total proportion of antigen-specific T cells than DyBs.

A proportion of 87% OT-I T cells was positive for both TIM-3 and PD-1 upon IB stimulation, which is higher than what we found for DyB-stimulated OT-I T cells (18.9%) (Figure 5f; Figure S8b–e, Supporting Information). Notably, IB incubation in IL-7 resulted in only 20% of double positive cells, which complements our previous observation that the choice of exogenously supplied cytokine can affect the phenotype of expanded cells (Figure S9e, Supporting Information). While TIM-3 and PD-1 are often used as markers to indicate exhaustion, various reports have been published that debate the use of PD-1 and TIM-3 alone to determine T cell exhaustion.[23] To further investigate the functionality of the IB- and DyB-expanded T cells, we looked into co-expression of effector markers. Upon restimulation with PMA and Ionomycin, ≈77% of IB-stimulated OT-I T cells expressed 3 or more effector markers, which is comparable to DyB-stimulated OT-I T cells (61%). (Figure 5g; Figure S8f–i, Supporting Information).

To investigate if the IB- and DyB- expanded OT-I T cells retain their cytotoxic capabilities, we co-cultured our expanded $CD8^+$ T cell products with $B16^{OVA}$ and OVA-negative B16 cells. Notably, the $CD8^+$ T cell population consisted of both $CD45.1^+$ T cells and $CD45.2^+$ OT-I T cells. When expanded with IBs, T cells lysed 22% $B16^{OVA}$ cells in a 2:1 effector: target ratio, while DyB-expanded T cells only lysed 6% (Figure 5h). This is likely due to the higher portion of OT-I T cells present within the $CD8^+$ population after expansion with IBs (Figure 5b,c). Additionally, the higher percentage of lysis by IB-treated $CD8^+$ T cells could also be attributed

13 f) of OT-I T cells. g,h) Frequency of OT-I T cells in the culture on day 7 and day 13 g) after stimulation with IBs or DyBs and representative flow plots h). i,j) Memory phenotype OT-I T cells based on CD44 and CD62L staining 7 days i) or 13 days j) after stimulation with IBs or DyBs. k) Frequency of cells positive for the expression of both PD-1 and TIM-3 on day 13 after stimulation with IBs or DyBs. l) Expression of effector markers TNFα, IFNγ, CD107a and IL-2 after restimulation of OT-I T cells. Pie charts show the % of cells positive for 0,1,2,3, or 4 markers. The arcs represent the different markers. Statistical significance was tested with one-way ANOVA on non-transformed (d) or two way-ANOVA on log-transformed (e,f), or non-transformed g,i,j) data with post-hoc Sidak's multiple comparison test or unpaired t-test k). $n = 3$ in three independent experiments.

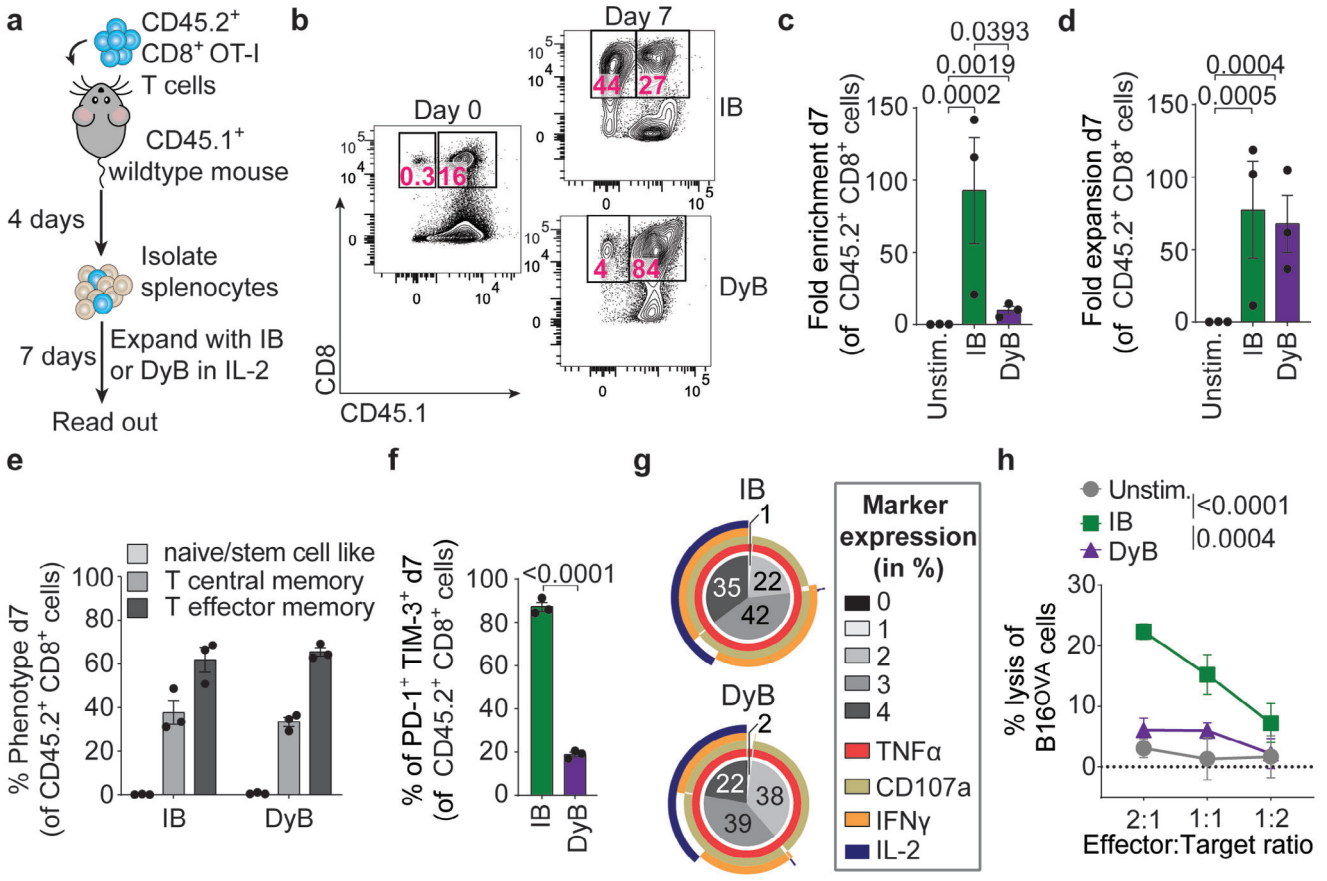

Figure 5. IBs enrich and expand antigen-specific T cells within splenocytes. a) Schematic workflow. b) Representative flow plot on day 0 after isolation of splenocytes and on day 7 after expansion with IBs or DyBs. Pink numbers in squares indicate the percentage of either the viable antigen-specific OT-I T cell population ($CD8^+$ $CD45.1^-$) or the viable wildtype antigen-nonspecific T cell population ($CD8^+$ $CD45.1^+$). c,d) Fold enrichment c) and fold expansion d) of antigen-specific OT-I T cells from day 0 to day 7 with IBs or DyBs. e) Proportion of the different memory phenotypes of antigen-specific cells after 7 days of stimulation with IB or DyB. f) Expression of the exhaustion markers PD-1 and TIM-3 on day 7. g) Expression of effector markers TNFα, CD107a, IFNγ, and IL-2 after restimulation. Pie charts show the % of cells positive for 0,1,2,3, or 4 markers. The arcs represent the different markers. h) Percentage of specific lysis of $B16^{OVA}$ target cells after overnight incubation with $CD8^+$ T cells isolated after 7 days of expansion from splenocytes with IBs, DyB or left unstimulated. Statistical significance was determined with one-way ANOVA on log-transformed data (c,d) with post-hoc Tukey's multiple comparison test, or unpaired t-test (f) or two-way ANOVA (e,h) with post-hoc Sidak's (e) or Tukey's (h) multiple comparison test. $n = 3$ in one experiment.

to a higher expression of cytotoxic effector markers (Figure 5g). At 2:1 effector: target ratios, ≈8% of the OVA-negative B16 cells were lysed, which, similar to what we described previously, is possibly a result of non-specific cytotoxicity of IB-activated T cells (Figure S9j, Supporting Information).[18] Thus, we show that stimulation of T cells within splenocytes with IBs results in higher subsequent antigen-specific lysis of the $B16^{OVA}$ target cells compared to stimulation with DyBs. Together, our findings demonstrate that IBs are very well capable of stimulating small populations of antigen-specific cells. More strikingly, IBs allow to rapidly enrich and expand antigen-specific T cells from a diverse population of cells, obviating the need for prior enrichment through magnetic columns or on feeder cell layers. Most of the IB-stimulated OT-I T cells acquire a T_{em} phenotype after 7 days and express multiple effector molecules. In addition, the IB-expanded OT-I T cells show excellent abilities to lyse target cells, indicating that the expanded T cells remain functional after 7 days of stimulation with IBs.

3. Conclusion and Outlook

In this work, we have developed an IB platform for efficient and selective expansion of antigen-specific OT-I T cells ex vivo. We hypothesize that our platform effectively stimulates T cells due to the semi-flexibility of the polymer brushes that facilitate receptor rearrangement on the T cell. Using our IB system, we can rapidly generate large numbers of antigen-specific T cells, even from remarkably low starting populations from as little as 0.1–0.01%, within non-specific T cells or splenocytes. We have determined the optimal design of our IBs and demonstrated the imperative role of the polymer scaffold in T cell stimulation. By systematically varying immunomodulator combinations on the IBs, we found that IBs decorated with at least pMHC and αCD28 effectively expanded highly functional OT-I T cells that retained their tumor cell killing ability. The T cells were mainly central memory cells, showed limited exhaustion markers and increased expression of multiple effector markers, indicating tumor-killing

capabilities. Furthermore, we demonstrate that both IF concentration and bead to cell ratio are critical parameters for T cell stimulation, which can be precisely controlled with our platform.

Many aAPC-designs for antigen-specific T cell expansion comprise spherical rigid scaffolds that do not facilitate clustering of the TCR[11j–l] and therefore stimulate T cells suboptimally.[7a,11o] To improve interaction with T cells, aAPCs have been developed with optimized particle size,[11m,24], shape,[7b,9,11o] or improved spacing of the stimulation signals.[25] These aAPCs showed promising results, with some currently being used in the clinic.[26] Nonetheless, none of them facilitate dynamic rearrangement of TCR clusters, which is a critical step for the T cells–natural APC interaction. Recently, membrane-mimicking lipid vesicle-based aAPCs have been designed to support microclustering by embedding signals in a fluid surface.[11a] While the T cell-stimulating capabilities of these aAPCs are impressive, their generation and subsequent separation from cells is laborious. Our IB system unifies a semi-flexible scaffold to facilitate receptor rearrangement with a magnetic core that can be easily removed from cell culture. The modular design of the IB system provides a high level of versatility, that allows to determine the optimal IB composition for a desired application by systemically combining different variations of IFs. As the IFs can be stored frozen, IBs can be generated on demand, resulting in an "off-the-shelf" platform.

Our findings show that IBs provide a promising platform for antigen-specific expansion of T cells ex vivo. The modular design of the IBs facilitates easy extrapolation of the platform to relevant therapies, such as stimulation of TILs. ACT with expanded TILs has shown positive results in patients with metastatic melanoma.[2a,27] Recent studies suggest that expansion and the breadth of neo-epitope specific $CD8^+$ T cells is essential for successful ACT of expanded TILs.[28] Additionally, expanding T cells that only recognize tumor-specific neoantigens can minimize side effects related to ACT.[29] As such, translation of our IB platform toward expansion of neo-antigen recognizing T cells would be highly interesting.

4. Experimental Section

Synthesis of Biotin End-Functional PIC: Biotin end-functional PIC was synthesized according to the previously reported protocol.[13] In short, PICs comprising a first block with allyl groups and a second block with azide groups were synthesized. To this end, allyl-, azide-, and methoxy-terminated isocyanide monomers were prepared as described in literature.[12,13] For the synthesis of the first block, allyl-terminated and methoxy-terminated isocyanide monomers were dissolved in a 1:1 molar ratio in dry toluene (27.7 mM), obtained from a MBraun SPS 800 solvent system. A 4 mM catalyst solution ($Ni(ClO_4)_2 \cdot 6H_2O$ in EtOH: toluene, 9:1, v/v) was added with a catalyst: monomer ratio of 1:100. The resulting mixture was reacted for 10 min at room temperature (rt). Next, for the synthesis of the second block, a solution of azide-terminated monomer (1.47 mg, 0.00395 mmol) and methoxy-terminated monomer (46.1 mg, 0.128 mmol) in dry toluene (1.19 ml) was added to the reaction mixture and stirred overnight at rt. Complete isocyanide consumption was confirmed by the disappearance of the characteristic FT-IR peak at 2140 cm^{-1}. The polymers were precipitated three times in cold (0 °C) diisopropylether and dried overnight to yield an off-white solid (32.2 mg, 64.4%). The average polymer length, polydispersity index and molecular weight were determined using AFM (Nanoscope IV Bruker, NSG-10 tapping mode tips, NT-MDT) and were found to be 219 ± 111 nm (SEM, Figure S1a,b, Supporting Information), 1.25 and 687 kg mol^{-1}, respectively. The characteristic helical backbone of the PICs was confirmed by Circular Dichroism (CD) spectroscopy of PIC solutions in PBS (pH 7.4) (Figure S2, Supporting Information).[30] Finally, the allyl groups in the first block were biotinylated via the NITEC reaction using tetrazole-PEG_8-biotin similar to the procedure described before.[13] Briefly, tetrazole-PEG_8-biotin was dissolved in PBS (0.7 mM, 0.060 ml), degassed through bubbling of N_2 and transferred into a quartz cuvette. The cuvette was placed in a dewar under a 254 nm lamp (Camag) and irradiated for 1 h. 0.30 mL of a 2.0 mg ml^{-1} solution of the allyl end-functional PIC in PBS was added to the activated tetrazole solution and incubated overnight on the rotation mixer at rt. After the reaction, 25 µl of the solution was diluted to 0.25 mg ml^{-1} in PBS and fluorescence was measured on a plate reader (Tecan Spark M10, ex: 368 nm, em: 514 nm) to confirm formation of the fluorescent pyrazoline ring. The biotin end-functional PIC was then labeled with Cyanine 7 (Cy7) through addition of dibenzocyclooctyne (DBCO)-conjugated Cy7 (Click Chemistry Tools) in a 1:500 dye:monomer ratio, followed by incubation at rt for 1 h. The resulting fluorescently labeled BiotinPIC was used without purification.

MHC Production: MHC complexes were prepared as described by Luimstra et al.[31] Heavy chains (H2-Kb) and human beta-2-microglobulin (hβ2m) were produced in a form of inclusion bodies in *E.coli* BL21(DE3)pLysS using T7 RNA polymerase/promoter system.[32] Isolated inclusion bodies were solubilized in denaturing buffer (8 M urea/100 mM Tris•Cl, pH 8). hβ2m was pre-folded in dialysis against 10 mM Tris•Cl (pH 7) in PBS. To prepare the final MHC complex, hβ2m and heavy chain were dissolved to final concentrations of 6 and 3 mM respectively in folding buffer (100 mM Tris•Cl, pH 8; 400 mM L-arginine; 2 mM EDTA; 5% glycerol; 5 mM reduced glutathione; 0.5 mM oxidized glutathione; Protease Inhibitor Cocktail, Roche Diagnostics) with 60 mM template peptide (SIINFEKL; GenScript). The folding reaction was incubated at 10 °C for 5 days. After filtration, concentration and buffer exchange to PBS, the complexes were purified via Size Exclusion Chromatography using a HiLoad 16/600 Superdex 75pg column (Cytiva). Ready MHC complexes were analyzed using SDS-PAGE and NanoDrop, concentrated, snap-frozen and stored at −80 °C until further use.

Functionalization of Immunomodulators: Anti-mouse αCD28 (clone 37.51, BioXcell), recombinant human IL-2 (ProSpec Bio) and MHC loaded with SIINFEKL were functionalized with DBCO or biotin and fluorescent dyes as described previously.[11f,g,30] To assure equal dye labeling among the DBCO-functionalized biomolecules and their biotin-functionalized counterparts, the immunomodulators were labeled with dye first. For αCD28, the antibody storage buffer was converted to 50 mM borate buffer pH 8.5 using Amicon centrifugal filters (30 MWCO, Merck). The pMHC and IL-2 were dissolved in PBS and Milli-Q, respectively. The immunomodulators were reacted with 3 eq Alexa Fluor 647-NHS ester (AF647, Thermo Fischer Scientific, for αCD28), 3 eq AzDye 405-NHS ester (A405, Click Chemistry Tools, for IL-2) or 2.5 eq Atto 488-NHS ester (A488, Atto-TEC GMbH, for pMHC) and reacted for 2 h at 4 °C. The batches of dye-functionalized immunomodulator were split, and half was reacted with 4 eq (for αCD28 and IL-2) or 3 eq (for pMHC) DBCO-PEG_4-NHS (Jena Bioscience), while the other half was reacted with 4 eq (for αCD28 and IL-2) or 3 eq (for pMHC) Biotin-PEG_4-NHS (Jena Bioscience) for 2 h at 4 °C. The functionalized immunomodulators were purified using Amicon centrifugal filters (30 MWCO, for αCD28; 10 MWCO, for IL-2 and pMHC, Merck). The degree of labeling (DOL) of DBCO and fluorescent dyes was determined using a NanoDrop 2000c spectrophotometer. The concentrations of immunomodulator, DBCO and dye were calculated based on the absorbance at wavelengths of 280, 309, 400, 501, and 650 nm and corrected for overlap in the absorbance spectra of the individual molecules. The DOL of DBCO was determined to be 1–2 and the DOL of the dyes was 1–3.

Conjugation of DBCO-Functionalized Immunomodulators to PIC: Biotin end-functional PIC in PBS (88.7 µl, 120 µg, 9.52 nmol azide monomer) was added to a mixture of DBCO functionalized pMHC (0.3 eq irt azide, 137 µg, 2.86 nmol), and/or αCD28 (0.3 eq irt azide, 429 µg, 2.86 nmol), and/or IL-2 (0.3eq irt azide, 148 µg, 2.86 nmol) in PBS and adjusted with PBS to reach a final concentration of 0.2 mg PIC per ml. The mixture was reacted at rt for 5 h, cooled to 4 °C and reacted for another 19 h. To

prevent cross-linking of PIC in the following steps, excess unreacted DBCO on the immunomodulators was quenched by addition of 1000 eq azido-PEG_3-amine (Conju-Probe). The resulting mixture was incubated for 1 h at rt. The functionalized PICs, when used for grafting, were then used without further purification. When used for determination of the amount of the immunomodulator per PIC, the conjugated PICs were purified using affinity purification, as described previously.[30] The immunomodulator spacing on the PIC was determined by measuring the fluorescence of the corresponding labels on the PIC, pMHC, αCD28, and IL-2 and comparing it to the standard curves of the pure labeled compounds (Table S1, Supporting Information).

Synthesis of Immunobrushes and Direct Beads: Streptavidin-coated magnetic beads were prepared from 4.5 µm diameter beads with a tosyl-activated surface (Dynabeads M-450 Tosylactivated, Thermo Fisher Scientific). A tosyl bead suspension (0.500 ml) was washed three times with 50 mM borate buffer pH 8.5 using a magnetic rack (Westburg BV). The tosyl beads were resuspended in 20 µM Streptavidin in borate buffer (0.500 ml, 50 mM, pH 8.5) and reacted for 16 h at rt. The beads were washed three times with 0.05% PBS Tween, three times with PBS and resuspended in PBS containing 0.01% BSA. For the preparation of IBs and DirectBs, the streptavidin-coated beads were incubated with the desired amount of biotin end-functional PIC or biotin-functionalized immunomodulators, respectively. The beads were incubated with the desired biotin-functionalized compounds on a rotator for 68 h at 4 °C and washed three times with 0.05% PBS Tween, three times with PBS and resuspended in PBS containing 0.01% BSA and 0.05% NaN_3. The resulting IBs and DirectBs were analyzed by flow cytometry on a BD FACS Verse cytometer via a similar method as the previously described stripping assay.[13] Briefly, streptavidin beads were incubated with varying concentrations of the desired biotin-functionalized immunomodulator (αCD28 or pMHC). To determine the biomolecule concentration on the beads, αCD28-functionalized and pMHC-functionalized direct beads were subjected to a stripping assay. DirectBs (30 µl) were suspended in stripping solution (120 µl, 3 mM biotin in 2% SDS Milli-Q), reacted at 90 °C for 20 min and subsequently cooled on ice for 10 min. The beads and supernatant were separated using a magnetic rack (Westburg BV). Fluorescence of the supernatant (100 µl) was measured on a TECAN Spark M10 plate reader (ex: 635 nm, em: 682 nm for αCD28; ex: 485 nm, em: 535 nm for pMHC). The stripped DirectBs were washed three times with 0.05% PBS Tween, three times with PBS and resuspended in PBS. The MFI of the stripped beads and their corresponding DirectBs was measured by flow cytometry on a BD FACS Verse cytometer and used to determine the stripping yield. Combining the stripping yield together with the fluorescence of the supernatant afforded standard curves of immunomodulator (αCD28 or pMHC) concentration per million beads with corresponding MFI. For the flow cytometry analysis, single beads were gated using a plot of forward scatter versus side scatter, and the mean fluorescent intensities (MFIs) of the A405, A488, and AF647 labels were recorded using the V-450, FITC, and APC channel, respectively. Synthesis of the αCD28- and pMHC- DirectBs and corresponding stripping assays were carried out in duplo. A quantification overview of all IBs and DirectBs can be found in Table S2 (Supporting Information). In the case that multiple batches of IBs or DirectBs were used, the quantification was given as an average of those batches.

$CD8^+$ T Cell Isolation and Cell Culture: Wildtype $CD8^+$ T cells were isolated from B6.SJLPtprcaPepcb/BoyCrl//aka Ly5.1//aka CD45.1 mice (Charles River). OT-I $CD8^+$ T cells were isolated from OT-I aka C57BL/6-Tg(TcraTcrb)1100Mjb mice (Charles River). Double-transgenic dsRed OT-I $CD8^+$ cells were a kind gift of Dr. P. Friedl (Radboudumc, the Netherlands) and isolated as described.[33] Briefly, spleens and lymph nodes were harvested and digested in 20 µg ml^{-1} Dnase I (Roche, 11 284 932 001) and 1 mg ml^{-1} collagenase III (Worthington, LS004182) for 30 min at 37 °C. Organs were put through a 100 µm cell strainer. Erythrocytes were eliminated by in-house ammonium-chloride-potassium lysis buffer. $CD8^+$ T cells were isolated by negative selection using a $CD8^+$ T cell isolation kit (Miltenyi, 130-104-075). Cells were diluted to desired cell concentration in RPMI 1640 (Gibco, 42 401 042) supplemented with 10% Fetal Bovine Serum (FBS), 2 mM L-Glutamine (Lonza, Biowhittaker, BE17-605E/U1) and 1% Anti/Anti (Gibco, 15240-062) and 50 µM β-mercaptoethanol (βMe) (Gibco, 21 985 023). Cells used for proliferation studies were stained with 2.5 µM CellTrace Violet (CTV) (Invitrogen, C34557) or CellTrace Far Red (CTFR) (Invitrogen, C34572) in 1% FBS in 1xPBS for 10 min at 37 °C and subsequent recovery for 30 min in 50% FBS at 37 °C. Cells were washed in 1xPBS and diluted to desired concentration in cell culture medium. If $CD8^+$ cells were cultured to determine the phenotype after 7 and 13 days, medium was supplemented with 300 U ml^{-1} recombinant human Interleukin-2 (Proleukin, Novartis) unless otherwise indicated. Cells were split regularly.

B16F10 and B16F10-ovalbumin ($B16^{OVA}$) expressing melanoma cell lines were cultured in cell culture medium without βMe. The medium for $B16^{OVA}$ was supplemented with 1 mg ml^{-1} Geneticin (Gibco, 11 811 064) and 60 µg ml^{-1} Hygromycin B (Gibco, 10 687 010). All cells were cultured at 5% CO_2, 37 °C in humidified atmosphere.

Dendritic Cell Generation and Cell Culture: Femur and tibia of wildtype B6.SJLPtprcaPepcb/BoyCrl//aka Ly5.1//aka CD45.1 mice (Charles River) were collected. Bone marrow was washed out onto a 100 µm cell strainer, cells were washed and plated in 10 cm petri dish (Greiner, 633 185) in supplemented cell culture medium as described above. The RPMI medium was additionally supplemented with 200 ng ml^{-1} human Flt3 ligand (Miltenyi, 130-096-479) and 5 ng ml^{-1} murine GM-CSF (Peprotech, 315-02) and 50 µM βMe. Cells were cultured at a density of 15×10^6 per plate at 10% CO_2, 37 °C in humidified atmosphere. After 5 days, medium was replaced with fresh 200 ng ml^{-1} Flt3 ligand and 5 ng ml^{-1} murine GM-CSF. After 9 days, cells were harvested, counted, and replated, and 200 ng ml^{-1} fresh Flt3 ligand and 5 ng ml^{-1} GM-CSF containing medium was added up to 10 ml. One day before T cell co-culture, cells were stimulated with 0.3 µg ml^{-1} LPS (vac-3pelps, invivogen). On the day of T cell co-culture, cells were given 100 ng ml^{-1} SIINFEKL (Genscript) peptide for 3 h. After 3 h, cells were counted and diluted to desired concentration. Cells were co-cultured with 500000 $CD8^+$ OT-I T cells in a 48-well plate and from then on cultured at 5% CO_2, 37 °C in humidified atmosphere.

Bead Stimulation of T cells: IBs, DirectBs, or DyBs (Gibco, 11452D) were washed 3x in PBS (some with 10% Anti/Anti) in 1.5 ml Eppendorf tubes using the magnetic rack. Beads were diluted in supplemented cell culture medium to the desired concentration and added to the corresponding plate after resuspension.

Cytokine Levels in Supernatant: Supernatant of cell cultures from different culture times was stored at −20 °C until Enzyme linked immunosorbent assays (ELISAs) were conducted to determine cytokine levels. IFNγ levels, IL-2 levels and, TNFα levels were measured using the Mouse IFNγ Uncoated ELISA Kit (ThermoFisher, 88-7314-76), or IL-2 Mouse Uncoated ELISA Kit (ThermoFisher, 88-7024-76) or TNFα Mouse Uncoated ELISA Kit (ThermoFisher, 88-7324-77) following the manufacturer's instructions. Plates were read on BioRad plate reader at a wavelength 450 nm and subtracted by 595 nm.

Flow Cytometry and Cell Sorting: Cells were resuspended and transferred to a V-bottom plate. For restimulation, cells were treated with 20 ng ml^{-1} PMA (Calbiochem, 524 400) and 1 µg ml^{-1} Ionomycin (Merck, I0634) in the presence of 10 µg ml^{-1} Brefeldin A (Cayman Chemical, 11861-25) and 1:1000 Monensin (eBioscienceTM, 00-4505-51) for 5.5 h in a V-bottom plate. Cells were washed (300 xg for 3 min, 4C) 1x in PBS and stained for viability with 1:2000 eFluor 780 fixable viability dye (eBioscience, 65-0865-14) or Zombie dye (Biolegend, 423 113) for 15 min in the dark at 4 °C. Cells were washed 1x in Protein Blocking Agent (PBA). For staining, the following antibodies were used: anti-CD3-APC-Cy7 (clone: 17A2,Biolegend, 100 221), anti-CD3-FITC (clone: 17A2,Biolegend 100 204,), anti-CD8a-PE (clone: 53.6-7, BDPharmingen, 553 033), anti-CD8-FITC (clone: 53–6.7, 553 031, BDPharmingen), anti-CD16/anti-CD32 Fc block (clone: 2.4G2, BDPharmingen, 553 142,) anti-CD25-PECy7 (clone: PC61, Biolegend, 102 016), anti-CD45.1-PerCp (clone: A20, Biolegend, 110 726), anti-CD44-PE-Cy7 (clone: IM7, Biolegend, 103 030), anti-CD62L-PerCp (clone: MEL-14, Biolegend, 104 429,), anti-CD62L-BV510 (clone: MEL-14, Biolegend, 104 441), anti-CD69-BV510 (clone: H1.2F3, Biolegend, 104 532), anti-CD279-PE (clone: 29F.1A12, Biolegend, 135 206), anti-CD279-APC (clone:29F.1A12, Biolegend, 135 209), anti-TIM3-BV421 (clone: RMT3-23, Biolegend, 119 723), anti-IFNγ-BV510 (clone: XMG1.2,

Biolegend, 505 841,), anti-IL-2-PE (clone: JES6-5H4, Biolegend, 503 808,), anti-IL-2-V450 (clone:JES6-5H4, Biolegend, 503 825), anti-CD107a-A647 (clone: 1D4B, Biolegend, 121 610), anti-TNFα-PECy7 (clone: MP6-XT22, Biolegend, 506 324).

Cells were washed 2x in PBA or 2x in PBS and then acquired on BD FACS Verse, BD FACS Lyric or MACSQuant. Viability dye 7-AAD (1:100, eBioSciences, 00-6993-50) was added shortly before acquisition to some samples. Compensation was done using ABC Compensation beads (invitrogen, A10497), and corresponding fluorescence minus one samples were taken along where necessary. The number of cells was evaluated by adding Precision counting beads (Biolegend, 424 902).

For sorting, cells were stained as described above. Viable cells were sorted on the BD FACSMelody into polypropylene tubes based on positive expression of CD8 and CD45.2 and no expression of CD45.1. Subsequently, cells were counted and diluted to desired concentration. Buffers used to wash and stain the cells did not contain sodium azide and were sterile.

In Vitro Target Cell Killing Assay: To test the killing capacity of pure antigen-specific OT-I T cells, 500000 OT-I $CD8^+$ T cells were cultured for two weeks in a 48-well plate with a 1:1 ratio of T cells to beads (IB, DirectB, DyB), 5:2 ratio of T cell to DC or left unstimulated. On day 13 of T cell expansion, beads were removed with a magnetic rack and cells were sorted as described above. On the same day, overnight IFNγ-pretreated (100 ng ml^{-1} (peprotech, 315-05) B16 ($B16\text{-}F10^{OVA}$ and B16-F10) were stained with either CTV or Carboxyfluorescein succinimidylester (CFSE), respectively, and mixed in a 1:1 ratio. The mixture of B16 cells was seeded in a 96 U-bottom well plate at a density of 20000 cells per well in cell culture medium for T cells. B16 cells were left to attach for 2 h, then effector cells were added in different effector to target ratios.

To test the killing capacity of enriched antigen-specific effector cells within a $CD8^+$ T cell population, 1 million splenocytes, containing OT-I $CD8^+$ T cells, were cultured in 300 IU ml^{-1} IL-2 in a 24-well plate with either IBs, DyBs or left unstimulated. After one week, beads were magnetically removed from the splenocyte population. Subsequently, $CD8^+$ T cells were isolated and added in different effector to target ratios to the mixture of B16 cells ($B16\text{-}F10^{OVA}$ and B16-F10). B16 cells were seeded one day prior to effector cell addition, in a 96 U-bottom well plate at a density of 20000 cells per well. B16 cells were not pre-treated with IFNγ.

After 20 h, B16 cells and T cells were collected and stained for viability and CD8, and then fixed in 4% paraformaldehyde solution for 20 min. The % of specific lysis was calculated as follows:

% specific lysis = (1-(Freq. treated viable target cells/Freq. no T cell-treated viable target cells)) x 100

Mice: All mice used in the experiments were housed at the Central Animal Laboratory (Nijmegen, the Netherlands) in accordance with the European legislation. All conducted protocols were approved by the local authorities (CCD, The Hague, The Netherlands) for the care and use of animals with related codes of practice. Mice were housed in IVC greenline cages and were provided with ad libitum food and water and cage enrichment.

OT-I Cell Enrichment from Splenocytes: One million OT-I T cells were adoptively transferred via the intravenous route into wildtype B6.SJLPtprcaPepcb/BoyCrl//aka Ly5.1//aka CD45.1 mice (Charles River). Mice were sacrificed 4–5 days after adoptive cell transfer and the spleen was isolated and digested as described above. Next, 1×10^6 splenocytes were added to a 24-well plate and IBs or DyBs were added in a 1:1 ratio. Medium was supplemented with 10 ng ml^{-1} recombinant human IL-7 (Biolegend, 581 906) or 300 IU ml^{-1} recombinant human IL-2 (Proleukin, Novartis) and cells were split when appropriate. Cells were cultured for one week before read-out.

Statistics: All data were represented as mean ± standard error of the mean (SEM). Graphs were generated in GraphPad Prism (version 8.0.2) and SPICE (version 6.1).[34] Statistical analysis was performed on transformed data where appropriate, using GraphPad Prism with the appropriate testing methods as indicated in the figure legends. Statistical significance was defined as a two-sided significance level of <0.05. Only relevant p-values < 0.05 are indicated in the graphs.

Ethics Approval Statement: Mice were housed at the Central Animal Laboratory (Nijmegen, the Netherlands) in accordance with the European legislation. All conducted protocols were approved by the local and national authorities (CCD, The Hague, the Netherlands; license number 10300-2019-0020) for the care and use of animals with related codes of practice.

Supporting Information

Supporting Information is available from the Wiley Online Library or from the author.

Acknowledgements

L.G. and L.W., contributed equally to this work. The authors thank the central animal laboratory Nijmegen (CDL) for their contribution to the animal work. The authors would like to acknowledge Mireille Toebes and Ton N. Schumacher for providing the H-2 kb and hβ2m constructs and protocols. The authors would like to acknowledge Peter Friedl and Daan Smits for providing with dsRed OT-I cells. This work was supported by ERC Advanced grant ARTimmune (834 618), ERC Starting grant CHEMCHECK (679 921), Oncode Base fund and the Oncode TechDev fund (P2020-0038). This work received funding from the Ministry of Education, Culture and Science through the Institute of Chemical Immunology (NWO Gravitation program 024.002.009, ICI00024) and the Research Center for Functional Molecular Systems (NWO Gravitation program 024.001.035).

Conflict of Interest

C.F. is the chief scientific officer and co-founder of Simmunext biotherapeutics, which develops novel immunotherapies by mimicking immune cell function through its proprietary polymer platform technology. C.F. is an inventor on patent WO2012004369 (2012); C.F., and R.H. are inventors on patent WO2019154865 (2019); C.F., R.H. and M.V. are inventors on patent WO2020174041. The other authors declare no conflict of interest.

Data Availability Statement

The data that support the findings of this study are available from the corresponding author upon reasonable request.

Keywords

antigen-specific T cells, Immunobrushes, Immunofilaments, Immunotherapy, T cell expansion

Received: July 4, 2023
Revised: November 22, 2023
Published online: December 22, 2023

[1] M. W. Rohaan, S. Wilgenhof, J. B. A. G. Haanen, *Virchows Arch.* **2019**, *474*, 449.

[2] a) S. A. Rosenberg, J. C. Yang, R. M. Sherry, U. S. Kammula, M. S. Hughes, G. Q. Phan, D. E. Citrin, N. P. Restifo, P. F. Robbins, J. R. Wunderlich, K. E. Morton, C. M. Laurencot, S. M. Steinberg, D. E. White, M. E. Dudley, *Clin. Cancer Res.* **2011**, *17*, 4550; b) R. Andersen, M. Donia, E. Ellebaek, T. H. Borch, P. Kongsted, T. Z. Iversen, L. R.

Hölmich, H. W. Hendel, Ö. Met, M. H. Andersen, P. Thor Straten, I. M. Svane, *Clin. Cancer Res.* **2016**, *22*, 3734; c) L. T. Nguyen, S. D. Saibil, V. Sotov, M. X. Le, L. Khoja, D. Ghazarian, L. Bonilla, H. Majeed, D. Hogg, A. M. Joshua, M. Crump, N. Franke, A. Spreafico, A. Hansen, A. Al-Habeeb, W. Leong, A. Easson, M. Reedijk, D. P. Goldstein, D. Mccready, K. Yasufuku, T. Waddell, M. Cypel, A. Pierre, B. Zhang, S. Boross-Harmer, J. Cipollone, M. Nelles, E. Scheid, M. Fyrsta, et al., *Cancer Immunol. Immunother.* **2019**, *68*, 773; d) M. W. Rohaan, T. H. Borch, J. H. van dan Berg, Ö. Met, R. Kessels, M. H. Geukes Foppen, J. Stoltenborg Granhøj, B. Nuijen, C. Nijenhuis, I. Jedema, *N. Engl. J. Med.* **2022**, *387*, 2113.

[3] M O. Butler, N. Hirano, *Immunol. Rev.* **2014**, *257*, 191.

[4] a) R. Wu, M.-A. Forget, J. Chacon, C. Bernatchez, C. Haymaker, J. Q. Chen, P. Hwu, L. G. Radvanyi, *Cancer J.* **2012**, *18*, 160; b) C. Govers, Z. Sebestyén, M. Coccoris, R. A. Willemsen, R. Debets, *Trends Mol. Med.* **2010**, *16*, 77.

[5] a) L. J. Eggermont, L. E. Paulis, J. Tel, C. G. Figdor, *Trends Biotechnol.* **2014**, *32*, 456; b) C. Zheng, J. Zhang, H. F. Chan, H. Hu, S. Lv, N. Na, Yu Tao, M. Li, *Small Methods* **2021**, *5*, 2001191; c) C. J. Turtle, S. R. Riddell, *Cancer J.* **2010**, *16*, 374; d) A. Isser, N. K. Livingston, J. P. Schneck, *Biomaterials* **2021**, *268*, 120584.

[6] a) C. Smith, G. Økern, S. Rehan, L. Beagley, S. K. Lee, T. Aarvak, K. W. Schjetne, R. Khanna, *Clin. Transl. Immunol.* **2015**, *4*, 31; b) A. Trickett, Y. L. Kwan, *J. Immunol. Methods* **2003**, *275*, 251; c) Y. Shi, W. Wu, T. Wan, Y. Liu, G. Peng, Z. Chen, H. Zhu, *Int. Immunopharmacol.* **2013**, *15*, 129.

[7] a) R. Zappasodi, M. Di Nicola, C. Carlo-Stella, R. Mortarini, A. Molla, C. Vegetti, S. Albani, A. Anichini, A. M. Gianni, *Haematologica* **2008**, *93*, 1523; b) T. R. Fadel, F. A. Sharp, N. Vudattu, R. Ragheb, J. Garyu, D. Kim, E. Hong, N. Li, G. L. Haller, L. D. Pfefferle, S. Justesen, K. C. Herold, T. M. Fahmy, *Nat. Nanotechnol.* **2014**, *9*, 639.

[8] a) G. P. Linette, E. A. Stadtmauer, M. V. Maus, A. P. Rapoport, B. L. Levine, L. Emery, L. Litzky, A. Bagg, B. M. Carreno, P. J. Cimino, G. K. Binder-Scholl, D. P. Smethurst, A. B. Gerry, N. J. Pumphrey, A. D. Bennett, J. E. Brewer, J. Dukes, J. Harper, H. K. Tayton-Martin, B. K. Jakobsen, N. J. Hassan, M. Kalos, C. H. June, *Blood* **2013**, *122*, 863; b) R. A. Morgan, N. Chinnasamy, D. Abate-Daga, A. Gros, P. F. Robbins, Z. Zheng, M. E. Dudley, S. A. Feldman, J. C. Yang, R. M. Sherry, G. Q. Phan, M. S. Hughes, U. S. Kammula, A. D. Miller, C. J. Hessman, A. A. Stewart, N. P. Restifo, M. M. Quezado, M. Alimchandani, A. Z. Rosenberg, A. Nath, T. Wang, B. Bielekova, S. C. Wuest, N. Akula, F. J. Mcmahon, S. Wilde, B. Mosetter, D. J. Schendel, C. M. Laurencot, et al., *J. Immunother.* **2013**, *36*, 133.

[9] A. S. Cheung, D. K. Y. Zhang, S. T. Koshy, D. J. Mooney, *Nat. Biotechnol.* **2018**, *36*, 160.

[10] J. Oh, X. Xia, W. K. R. Wong, S. H. D. Wong, W. Yuan, H. Wang, C. H. N. Lai, Y. Tian, Y.-P. Ho, H. Zhang, Y. Zhang, G. Li, Y. Lin, L. Bian, *Small* **2022**, *18*, 2107373.

[11] a) J. Y. Chen, S. Agrawal, H. P. Yi, D. Vallejo, A. Agrawal, A. Lee, *Adv. Healthcare Mater.* **2023**, *12*, 2203163; b) X. Shou, Y. Yu, D. Wu, F. Wang, W. Sun, P. Duan, L. Shang, *Chem. Eng. J.* **2022**, *437*, 135374; c) Q.-V. Le, J. Lee, J. Byun, G. Shim, Y.-K. Oh, *Bioact. Mater.* **2022**, *15*, 160; d) S. Mandal, R. Hammink, J. Tel, Z. H. Eksteen-Akeroyd, A. E. Rowan, K. Blank, C. G. Figdor, *ACS Chem. Biol.* **2015**, *10*, 485; e) R. Hammink, S. Mandal, L. J. Eggermont, M. Nooteboom, P. H. G. M. Willems, J. Tel, A. E. Rowan, C. G. Figdor, K. G. Blank, *ACS Omega* **2017**, *2*, 937; f) L. J. Eggermont, R. Hammink, K. G. Blank, A. E. Rowan, J. Tel, C. G. Figdor, *Adv. Ther.* **2018**, *1*, 1800021; g) R. Hammink, J. Weiden, D. Voerman, C. Popelier, L. J. Eggermont, M. Schluck, C. G. Figdor, M. Verdoes, *ACS Appl. Mater. Interfaces* **2021**, *13*, 16007; h) D. K. Y. Zhang, K. Adu-Berchie, S. Iyer, Y. Liu, N. Cieri, J. M. Brockman, D. Neuberg, C. J. Wu, D. J. Mooney, *Nat. Commun.* **2023**, *14*, 506; i) K. Zhang, Y. Ma, D. Wang, J. Liu, J. An, Y. Li, C. Ma, Y. Pei, Z. Zhang, J. Liu, J. Shi, *Nano Lett.* **2022**, *22*, 1937; j) M. Oelke, M. V. Maus, D. Didiano, C. H. June, A. Mackensen, J. P. Schneck, *Nat. Med.* **2003**, *9*, 619; k) S. Ugel, A. Zoso, C. De Santo, Y Li, I. Marigo, P. Zanovello, E. Scarselli, B. Cipriani, M. Oelke, J. P. Schneck, V. Bronte, *Cancer Res.* **2009**, *69*, 9376; l) M. Oelke, J. P. Schneck, *Immunol. Res.* **2010**, *47*, 248; m) K. Perica, A. Tu, A. Richter, J. G. Bieler, M. Edidin, J. P. Schneck, *ACS Nano* **2014**, *8*, 2252; n) J. Ichikawa, T. Yoshida, A. Isser, A. S. Laino, M. Vassallo, D. Woods, S. Kim, M. Oelke, K. Jones, J. P. Schneck, J. S. Weber, *Clin. Cancer Res.* **2020**, *26*, 3384; o) J. C. Sunshine, K. Perica, J. P. Schneck, J. J. Green, *Biomaterials* **2014**, *35*, 269; p) E. Ben-Akiva, J. W. Hickey, R. A. Meyer, A. Isser, S R. Shannon, N. K. Livingston, K. R. Rhodes, A. K. Kosmides, T. R. Warren, S. Y. Tzeng, J. P. Schneck, J. J. Green, *Acta Biomater.* **2023**, *160*, 187.

[12] S. Mandal, Z. H. Eksteen-Akeroyd, M. J. Jacobs, R. Hammink, M. Koepf, A. J. A. Lambeck, J. C. M. Van Hest, C. J. Wilson, K. Blank, C. G. Figdor, A. E. Rowan, *Chem. Sci.* **2013**, *4*, 4168.

[13] D. Voerman, M. Schluck, J. Weiden, B. Joosten, L. J. Eggermont, T. Van Den Eijnde, B. Ignacio, A. Cambi, C. G. Figdor, P. H. J. Kouwer, M. Verdoes, R. Hammink, A. E. Rowan, *Biomacromolecules* **2019**, *20*, 2587.

[14] L. Gerrits, R. Hammink, P. H. J. Kouwer, *Polym. Chem.* **2021**, *12*, 1362.

[15] M. F. Mescher, *J. Immunol.* **1992**, *149*, 2402.

[16] a) T. N. J. Bullock, D. W. Mullins, V. H. Engelhard, *J. Immunol.* **2003**, *170*, 1822; b) P. A. González, L. J. Carreño, D. Coombs, J. E. Mora, E. Palmieri, B. Goldstein, S. G. Nathenson, A. M. Kalergis, *Proc. Natl. Acad. Sci. USA* **2005**, *102*, 4824; c) K. Perica, A. De León Medero, M. Durai, Y. L. Chiu, J. G. Bieler, L. Sibener, M. Niemöller, M. Assenmacher, A. Richter, M. Edidin, M. Oelke, J. Schneck, *Nanomed.: Nanotechnol. Biol. Med.* **2014**, *10*, 119; d) M. A. Alexander-Miller, G. R. Leggatt, A. Sarin, J. A. Berzofsky, *J. Exp. Med.* **1996**, *184*, 485.

[17] E. J. Wherry, *Nat. Immunol.* **2011**, *12*, 492.

[18] S. Ehl, J. Hombach, P. Aichele, H. Hengartner, R. M. Zinkernagel, *J. Exp. Med.* **1997**, *185*, 1241.

[19] a) M. E. Dudley, J. R. Wunderlich, P. F. Robbins, J. C. Yang, P. Hwu, D. J. Schwartzentruber, S. L. Topalian, R. Sherry, N. P. Restifo, A. M. Hubicki, M. R. Robinson, M. Raffeld, P. Duray, C. A. Seipp, L. Rogers-Freezer, K. E. Morton, S. A. Mavroukakis, D. E. White, S. A. Rosenberg, *Science* **2002**, *298*, 850; b) M. E. Dudley, J. Wunderlich, M. I. Nishimura, D. Yu, J C. Yang, S L. Topalian, D J. Schwartzentruber, P. Hwu, F. M. Marincola, R. Sherry, S F. Leitman, S. A. Rosenberg, *J. Immunother.* **2001**, *24*, 363.

[20] N. Kedia-Mehta, D. K. Finlay, *Nat. Commun.* **2019**, *10*, 2123.

[21] C. A. Klebanoff, L. Gattinoni, N. P. Restifo, *Immunol. Rev.* **2006**, *211*, 214.

[22] a) L. Gattinoni, C. A. Klebanoff, D. C. Palmer, C. Wrzesinski, K. Kerstann, Z. Yu, S. E. Finkelstein, M. R. Theoret, S. A. Rosenberg, N. P. Restifo, *J. Clin. Invest.* **2005**, *115*, 1616; b) M. C. Jensen, S. R. Riddell, *Immunol. Rev.* **2014**, *257*, 127.

[23] a) L. Avery, J. Filderman, A. L. Szymczak-Workman, L. P. Kane, *Proc. Natl. Acad. Sci. USA* **2018**, *115*, 2455; b) J. J. Hong, P. K. Amancha, K. Rogers, A. A. Ansari, F. Villinger, *PLoS One* **2013**, *8*, 60186; c) J. M. Jubel, Z. R. Barbati, C. Burger, D. C. Wirtz, F. A. Schildberg, *Front. Immunol.* **2020**, *11*, 487.

[24] J. W. Hickey, F. P. Vicente, G. P. Howard, H.-Q. Mao, J. P. Schneck, *Nano Lett.* **2017**, *17*, 7045.

[25] Y. Sun, J. Sun, M. Xiao, W. Lai, L. Li, C. Fan, H. Pei, *Sci. Adv.* **2022**, *8*, eadd1106.

[26] a) D. Langan, R. Wang, K. Tidwell, S. Mitiku, A. Farrell, C. Johnson, A. Parks, L. Suarez, S. Jain, S. Kim, K. Jones, M. Oelke, J. Zeldis, *Front. Med.* **2022**, *9*, 1070529; b) L. Suarez, R. Wang, S. Carmer, D. Bednarik, H. Myint, K. Jones, M. Oelke, *Transfus. Med. Hemother.* **2020**, *47*, 464.

[27] M. J. Besser, R. Shapira-Frommer, O. Itzhaki, A. J. Treves, D. B. Zippel, D. Levy, A. Kubi, N. Shoshani, D. Zikich, Y. Ohayon, D. Ohayon, B.

Shalmon, G. Markel, R. Yerushalmi, S. Apter, A. Ben-Nun, E. Ben-Ami, A. Shimoni, A. Nagler, J. Schachter, *Clin. Cancer Res.* **2013**, *19*, 4792.

[28] a) N. P. Kristensen, C. Heeke, S. A. Tvingsholm, A. Borch, A. Draghi, M. D. Crowther, I. Carri, K. K. Munk, J. S. Holm, A.-M. Bjerregaard, *J. Clin. Invest.* **2022**, *132*, 150535; b) J. S. Holm, S A. Funt, A. Borch, K. K. Munk, A.-M. Bjerregaard, J. L. Reading, C. Maher, A. Regazzi, P. Wong, H. Al-Ahmadie, G. Iyer, T. Tamhane, A. K. Bentzen, N. O. Herschend, S. De Wolf, A. Snyder, T. Merghoub, J. D. Wolchok, M. Nielsen, J. E. Rosenberg, D. F. Bajorin, S. R. Hadrup, *Nat. Commun.* **2022**, *13*, 1935.

[29] Z. Wang, Y. J. Cao, *Front. Immunol.* **2020**, *11*, 176.

[30] R. Hammink, L J. Eggermont, T. Zisis, J. Tel, C. G. Figdor, A E. Rowan, K G. Blank, *Bioconjugate Chem.* **2017**, *28*, 2560.

[31] J. J. Luimstra, K. L. M. C. Franken, M. A. Garstka, J. W. Drijfhout, J. Neefjes, H. Ovaa, *Curr. Protoc. Immunol.* **2019**, *126*, 85.

[32] S. Tabor, C. C. Richardson, *Proc. Natl. Acad. Sci. USA* **1985**, *82*, 1074.

[33] B. Weigelin, E. Bolaños, A. Teijeira, I. Martinez-Forero, S. Labiano, A. Azpilikueta, A. Morales-Kastresana, J. I. Quetglas, E. Wagena, A. R. Sánchez-Paulete, L. Chen, P. Friedl, I. Melero, *Proc. Natl. Acad. Sci. USA* **2015**, *112*, 7551.

[34] M. Roederer, J L. Nozzi, M. C. Nason, *Cytometry, Part A* **2011**, *79*, 167.